

# Dipolar spin ice states with fast monopole hopping rate in $\text{CdEr}_2\text{X}_4$ ( $X = \text{Se}, \text{S}$ )

Shang Gao,<sup>1,2</sup> O. Zaharko,<sup>1,\*</sup> V. Tsurkan,<sup>3,4</sup> L. Prodan,<sup>4</sup> E. Riordan,<sup>5</sup> J. Lago,<sup>6</sup> B. Fåk,<sup>7</sup> A. R. Wildes,<sup>7</sup> M. M. Koza,<sup>7</sup> C. Ritter,<sup>7</sup> P. Fouquet,<sup>7</sup> L. Keller,<sup>1</sup> E. Canévet,<sup>1,8</sup> M. Medarde,<sup>9</sup> J. Blomgren,<sup>10</sup> C. Johansson,<sup>10</sup> S. R. Giblin,<sup>5</sup> S. Vrtnik,<sup>11</sup> J. Luzar,<sup>11</sup> A. Loidl,<sup>3</sup> Ch. Rüegg,<sup>1,2</sup> and T. Fennell<sup>1,†</sup>

<sup>1</sup>Laboratory for Neutron Scattering and Imaging,

Paul Scherrer Institut, CH-5232 Villigen PSI, Switzerland

<sup>2</sup>Department of Quantum Matter Physics, University of Geneva, CH-1211 Geneva, Switzerland

<sup>3</sup>Experimental Physics V, University of Augsburg, D-86135 Augsburg, Germany

<sup>4</sup>Institute of Applied Physics, Academy of Sciences of Moldova, MD-2028 Chisinau, Republic of Moldova

<sup>5</sup>School of Physics and Astronomy, Cardiff University, CF24 3AA Cardiff, United Kingdom

<sup>6</sup>Department of Inorganic Chemistry, Universidad del País Vasco (UPV-EHU), 48080 Bilbao, Spain

<sup>7</sup>Institut Laue-Langevin, CS 20156, 38042 Grenoble Cedex 9, France

<sup>8</sup>Department of Physics, Technical University of Denmark, DK-2800 Kgs. Lyngby, Denmark

<sup>9</sup>Laboratory for Scientific Developments and Novel Materials,

Paul Scherrer Institut, CH-5232 Villigen PSI, Switzerland

<sup>10</sup>RISE Acreo AB, SE-411 33 Göteborg, Sweden

<sup>11</sup>Jožef Stefan Institute, SI-1000 Ljubljana, Slovenia

(Dated: June 13, 2021)

Excitations in a spin ice behave as magnetic monopoles, and their population and mobility control the dynamics of a spin ice at low temperature.  $\text{CdEr}_2\text{Se}_4$  is reported to have the Pauling entropy characteristic of a spin ice, but its dynamics are three-orders of magnitude faster than the canonical spin ice  $\text{Dy}_2\text{Ti}_2\text{O}_7$ . In this letter we use diffuse neutron scattering to show that both  $\text{CdEr}_2\text{Se}_4$  and  $\text{CdEr}_2\text{S}_4$  support a dipolar spin ice state – the host phase for a Coulomb gas of emergent magnetic monopoles. These Coulomb gases have similar parameters to that in  $\text{Dy}_2\text{Ti}_2\text{O}_7$ , *i.e.* dilute and uncorrelated, so cannot provide three-orders faster dynamics through a larger monopole population alone. We investigate the monopole dynamics using ac susceptometry and neutron spin echo spectroscopy, and verify the crystal electric field Hamiltonian of the  $\text{Er}^{3+}$  ions using inelastic neutron scattering. A quantitative calculation of the monopole hopping rate using our Coulomb gas and crystal electric field parameters shows that the fast dynamics in  $\text{CdEr}_2\text{X}_4$  ( $X = \text{Se}, \text{S}$ ) are primarily due to much faster monopole hopping. Our work suggests that  $\text{CdEr}_2\text{X}_4$  offer the possibility to study alternative spin ice ground states and dynamics, with equilibration possible at much lower temperatures than the rare earth pyrochlore examples.

A magnetic Coulomb phase is characterized by an effective magnetic field whose topological defects behave as emergent magnetic monopoles [1]. In dipolar spin ices such as  $\text{Dy}_2\text{Ti}_2\text{O}_7$ , where long-range dipolar interactions between spins on the pyrochlore lattice establish the two-in-two-out ice rule (which gives the field its non-divergent character) [2], the monopoles are deconfined and interact according to a magnetic Coulomb law [3–5]. The transformation from the spin model to a Coulomb gas of magnetic monopoles simplifies the understanding of the properties of dipolar spin ices as the complicated couplings among the spins are replaced by the determinant parameters of the Coulomb gas: the elementary charge  $Q_m$ , chemical potential  $v_0$ , and hopping rate  $u$  [3, 6]. Through analogs with Debye-Hückel theory of Coulomb gases, many thermodynamic observables can be conveniently calculated [7–9].

The spin relaxation rate of canonical spin ices was a particular problem in the spin representation. From high to low temperature it changes from thermally activated, to a temperature independent plateau, to a re-entrant thermally activated regime [10–13]. At high temperature, above the monopole regime, Orbach processes describe the thermally activated relaxation rate [13]. The

plateau and re-entrant thermally activated regimes are not readily explained in the spin representation, but can now be understood as the hopping of monopoles by quantum tunneling in screened and unscreened regimes of the Coulomb gas respectively [11, 12]. In the unscreened regime, the relaxation rate depends on the monopole density  $\rho$  with the hopping rate  $u$  as the coefficient:  $f \propto \rho u$  when the system is near equilibrium [7, 8, 14].

Although the monopole charge  $Q_m$  and chemical potential  $v_0$  can be calculated exactly from the spin model, the value of the monopole hopping rate  $u$  is not well-understood and is usually treated as a fitting parameter [11, 12, 15]. For  $\text{Dy}_2\text{Ti}_2\text{O}_7$ ,  $u$  is fitted to be  $\sim 10^3$  Hz at  $T < 12$  K, which has been experimentally confirmed through the Wien effect [6]. Recently, Tomasello *et al* found that this hopping rate can be estimated by the splitting of the crystal-electric-field (CEF) ground state doublet under an internal transverse magnetic field of 0.1–1 T [16]. To verify the universality of this approach, it is beneficial to compare the monopole dynamics in other dipolar spin ice compounds.

The newly proposed spin ice state in the spinel  $\text{CdEr}_2\text{Se}_4$  provides such an opportunity [17–19]. In this compound,  $\text{Er}^{3+}$  ions constitute the pyrochlore lattice,



peaks of  $\text{Er}_x\text{Se}_y$  impurities [20].

To fit the observed spin-spin correlations in  $\text{CdEr}_2\text{Se}_4$ , we performed single-spin-flip Monte Carlo simulations for the dipolar spin ice model with exchange couplings up to the second neighbors [29]:

$$\mathcal{H} = J_1 \sum_{\langle ij \rangle} \sigma_i \sigma_j + J_2 \sum_{\langle\langle ij \rangle\rangle} \sigma_i \sigma_j + D r_0^3 \sum_{ij} \left[ \frac{\vec{n}_i \cdot \vec{n}_j}{|r_{ij}|^3} - \frac{3(\vec{n}_i \cdot \vec{r}_{ij})(\vec{n}_j \cdot \vec{r}_{ij})}{|r_{ij}|^5} \right] \sigma_i \sigma_j. \quad (1)$$

Here,  $\vec{n}_i$  is the unit vector along the local  $\langle 111 \rangle$  axes with the positive direction pointing from one diamond sublattice of the tetrahedra center to the other,  $\sigma_i = \pm 1$  is the corresponding Ising variable,  $J_1$  and  $J_2$  are the exchange interactions for nearest neighbors (NN)  $\langle ij \rangle$  and second-nearest neighbors  $\langle\langle ij \rangle\rangle$ , respectively,  $r_0$  is the NN distance, and  $D = \mu_0 (\langle \hat{J}_z \rangle g \mu_B)^2 / (4\pi r_0^3)$  is the dipolar interaction, 0.62 and 0.69 K for  $\text{CdEr}_2\text{Se}_4$  and  $\text{CdEr}_2\text{S}_4$ , respectively. With the ALPS package [30], we implemented the Hamiltonian (1) on a  $6 \times 6 \times 6$  supercell with periodic boundary conditions. The dipolar interaction was truncated beyond the distance of 3 unit cells. The spin-spin correlations were evaluated every 100 sweeps during the  $4 \times 10^5$  sweeps of measurement. Assuming the effective NN coupling  $J_{\text{eff}} = J_1 + 5D/3$  to be equal to 1 K at which temperature the  $\text{CdEr}_2\text{Se}_4$  specific heat maximum was observed [18, 31, 32], we fixed  $J_1$  to  $-0.03(1)$  K and only varied  $J_2$  in the fitting process. As is shown in Fig. 2, the model with  $J_2 = 0.04(1)$  K fits the measured spin correlations very well. We found no need to include  $J_3$ , which appears in other dipolar spin ices [29]. Although the exact value of  $J_2$  might be susceptible to both the supercell size and the dipolar cutoff, our simulations do confirm the dominance of the dipolar interactions in  $\text{CdEr}_2\text{Se}_4$ . Non-polarized neutron diffuse scattering results for  $\text{CdEr}_2\text{S}_4$  are shown in the Supplemental Material [20], which have similar  $Q$ -dependence as that of  $\text{CdEr}_2\text{Se}_4$  and can be fitted by the dipolar spin ice model as well. In this way, we establish the existence of the dipolar spin ice state in  $\text{CdEr}_2\text{Se}_4$  and  $\text{CdEr}_2\text{S}_4$ .

With the fitted CEF ground states and coupling strengths, we can determine the monopole parameters. The monopole charge  $Q_m = 2\langle \hat{J}_z \rangle g \mu_B / \sqrt{3} 2r_0$  can be calculated to be 3.28 and  $3.42 \mu_B/\text{\AA}$  for  $\text{CdEr}_2\text{Se}_4$  and  $\text{CdEr}_2\text{S}_4$ , respectively [3]. The chemical potential  $v_0 = 2J_1 + (8/3)(1 + \sqrt{2/3})D$ , which is half of the energy cost to create and unbind a monopole-antimonopole pair [9], is 2.93 K for  $\text{CdEr}_2\text{Se}_4$  and 3.84 K for  $\text{CdEr}_2\text{S}_4$ . Although the chemical potentials in  $\text{CdEr}_2\text{X}_4$  are lower than that in  $\text{Dy}_2\text{Ti}_2\text{O}_7$  (4.35 K), they are still more than two times higher than the energy cost  $E_{\text{unbind}} = (8/3)\sqrt{2/3}D$  to unbind a monopole-antimonopole pair, locating both compounds in the same weakly correlated magnetolyte regime as  $\text{Dy}_2\text{Ti}_2\text{O}_7$  [9].

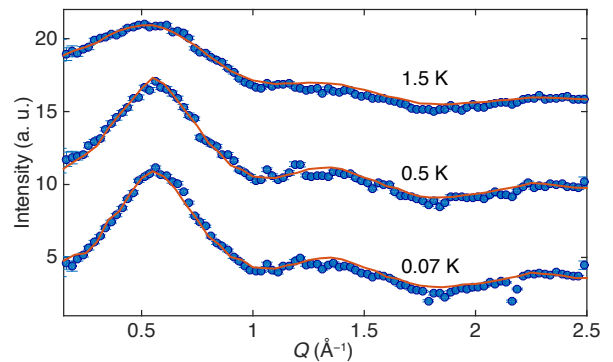


FIG. 2. (color online).  $\text{CdEr}_2\text{Se}_4$  magnetic scattering at 0.07, 0.5, and 1.5 K obtained from the  $xyz$  polarization analysis. The 0.5 (1.5) K data is shifted by 6 (12) along the  $y$  axis. The Monte Carlo simulation results are shown as the solid red lines.

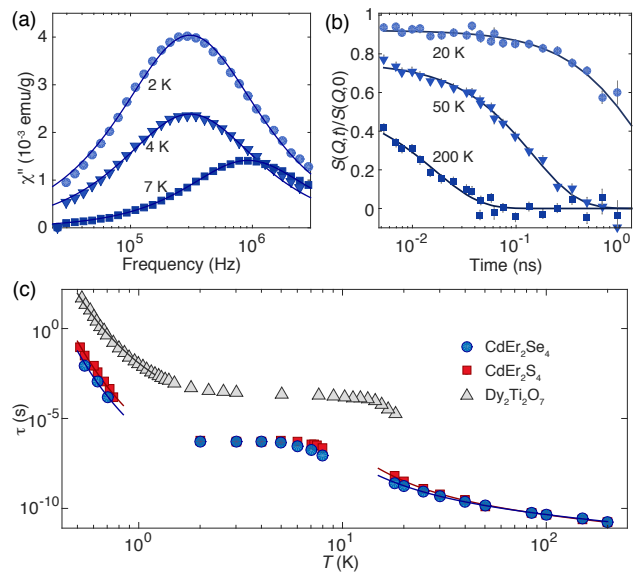


FIG. 3. (color online). (a) Imaginary parts of the ac susceptibilities of  $\text{CdEr}_2\text{Se}_4$  measured at 2, 4, and 7 K with the Cole-Cole model fits shown as the solid lines. (b) Normalized spin echo intermediate scattering function  $S(Q, t)/S(Q, 0)$  of  $\text{CdEr}_2\text{Se}_4$  measured at 20, 50, and 200 K with the fits shown as the solid lines. (c) Extracted relaxation time in  $\text{CdEr}_2\text{Se}_4$  and  $\text{CdEr}_2\text{S}_4$ . Error bars are smaller than the symbol sizes. The Arrhenius (Orbach) fits in the low (high) temperature regime are shown as the solid lines. Relaxation rates together with the low-temperature Arrhenius fits for  $\text{Dy}_2\text{Ti}_2\text{O}_7$  [33, 34] are shown for comparison.

Monopole dynamics in the low and high frequency regimes can be probed with ac-susceptibility [10, 33–35] and neutron spin echo spectroscopy [36, 37], respectively, and the representative results for  $\text{CdEr}_2\text{Se}_4$  are shown in Fig. 3a and b. Fig. 3c summarizes the temperature dependence of the characteristic relaxation time  $\tau = 1/2\pi f$  in  $\text{CdEr}_2\text{X}_4$ , where the results for  $\tau > 1 \times 10^{-3}$  s are extracted from the peak positions of the imaginary part









# Dipolar spin ice states with fast monopole hopping rate in $\text{CdEr}_2\text{X}_4$ ( $X = \text{Se}, \text{S}$ ) Supplementary Information

## Sample preparation

The polycrystalline samples of  $\text{CdEr}_2\text{X}_4$  ( $X = \text{Se}, \text{S}$ ) were prepared by solid state synthesis from binary Er and Cd selenides and sulfides. The binary  $\text{CdX}$  were synthesized from the elemental Cd-114, while the  $\text{Er}_2\text{X}_3$  were prepared from the high purity Er chips (99.9 %, Chempur) and elemental S (99.999 %, Strem Chemicals) or Se (99.999 %, Alfa Aesar). Selenium was additionally purified by zone melting. To reduce the oxide impurity  $\text{Er}_2\text{O}_2\text{X}$  which easily forms in the open air, all preparation procedures (quartz ampoule filling, reacted mixture regrinding, and pellets pressing) were performed in an argon box with an  $\text{O}_2$  and  $\text{H}_2\text{O}$  content of  $\sim 1$  ppm. To reach full homogeneity, at least three sintering cycles of synthesis of the binary Er and Cd chalcogenides were performed. The phase purity of the binary compounds was checked by x-ray powder diffraction. Finally, the ternary  $^{114}\text{CdEr}_2\text{X}_4$  were prepared by two consecutive synthesis at  $800^\circ\text{C}$  for one week each.

The single crystals of  $\text{CdEr}_2\text{X}_4$  were grown by the chemical transport reactions method. As starting materials the preliminary synthesized polycrystalline powders were used. For the growth, several transport agents were probed, including chlorine, bromine and iodine. We found that only the iodine is suitable for the growth of the ternary phase, while in the case of chlorine or bromine the final product contained mainly binary Cd and Er chalcogenides. The growth process was performed in a two-zone furnace with the hot part temperature of  $950^\circ\text{C}$  and a temperature gradient of about  $40^\circ\text{C}$ . The time for one crystal growth experiment was between 1 and 1.5 months. As a result, the octahedron-like single crystals with dimension up to 1.5 mm of the edge were obtained.

## Sample characterizations and impurities in $\text{CdEr}_2\text{Se}_4$

The purity content and crystal structure of the samples were checked by conventional X-ray powder diffraction on polycrystalline samples and crashed single crystals. Fig. S1 shows the refinement results for the  $^{114}\text{CdEr}_2\text{Se}_4$  and  $^{114}\text{CdEr}_2\text{S}_4$  polycrystalline samples using cubic  $Fd\bar{3}m$  symmetry expected for the normal spinel structure. Tab S1 lists the refined size of the unit cell, fractional position for the Se or S ions, and the goodness-of-fit parameters. No inversion between Cd and Er can be observed. No peaks from impurities are detectable, implying their tiny amount. However, at low temperatures, weak magnetic Bragg peaks of the  $\text{Er}_x\text{Se}_y$  impurities [S1] are discernible in the neutron diffuse scattering experiment shown in Fig. 2 of the main text.

The extrinsic origin of the weak Bragg peaks is evident in their different temperature dependence compared with the broad diffuse scattering. Fig. S2 shows the non-polarized neutron diffraction results measured on D20 at ILL with the 20 K measurement subtracted as the background. The setup with  $2.41 \text{ \AA}$  incoming neutron wavelength was employed. As can be seen in the inset of Fig. S2a and Fig. S2b, intensities of the sharp peaks saturate at temperatures below 0.8 K while the broad peaks from the diffuse scattering continue their growth, evidencing their different origins.

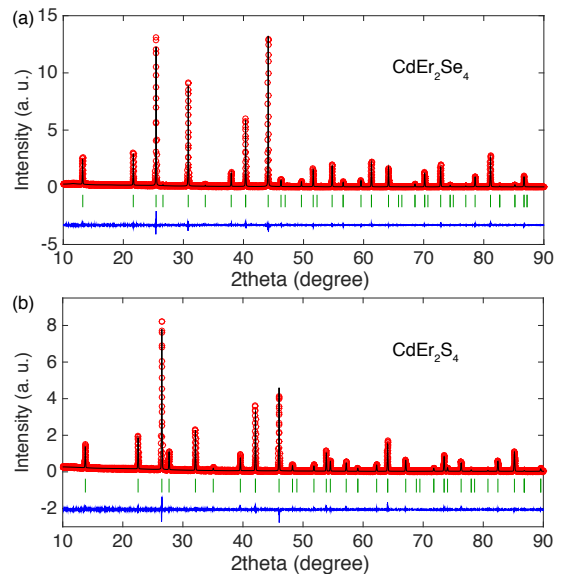


FIG. S1. Refinement results of the X-ray diffraction data measured at room temperature for (a)  $^{114}\text{CdEr}_2\text{Se}_4$  polycrystalline sample and (b)  $^{114}\text{CdEr}_2\text{S}_4$  polycrystalline sample. Data points are shown as red circles. The calculated pattern is shown as black solid line. The vertical bars mark the positions of Bragg peaks. And the blue line at the bottom shows the difference of data and calculated intensities.

TABLE S1. Refinement results of the X-ray diffraction data for  $\text{CdEr}_2\text{Se}_4$  and  $\text{CdEr}_2\text{S}_4$ . The listed parameters are the refined size of the unit cell  $a$ , fractional position  $x$  of the  $X = \text{Se}$  or  $\text{S}$  ions, and the goodness-of-fit  $R_p$ ,  $R_{wp}$ , and  $\chi^2$ .

	$a$ ( $\text{\AA}$ )	$X$ ( $x$ )	$R_p$	$R_{wp}$	$\chi^2$
$\text{CdEr}_2\text{Se}_4$	11.6097(1)	0.2566(1)	13.0	14.6	2.16
$\text{CdEr}_2\text{S}_4$	11.1527(1)	0.2589(2)	19.7	19.1	1.89





are shown in Fig. S3, and the ground states are:

$$\begin{aligned}
\text{Dy}^{3+} |\pm\rangle &= 0.176|15/2, \pm 13/2\rangle \mp 0.350|15/2, \pm 7/2\rangle \\
&\quad + 0.273|15/2, \pm 1/2\rangle \pm 0.554|15/2, \mp 5/2\rangle \\
&\quad + 0.682|15/2, \mp 11/2\rangle, \\
\text{Ho}^{3+} |\pm\rangle &= 0.157|8, \pm 8\rangle \mp 0.456|8, \pm 5\rangle \\
&\quad + 0.252|8, \pm 2\rangle \pm 0.096|8, \mp 1\rangle \\
&\quad + 0.743|8, \mp 4\rangle \pm 0.377|8, \mp 7\rangle, \\
\text{Tm}^{3+} |\phi\rangle &= 0.659|6, \pm 6\rangle \pm 0.200|6, \pm 3\rangle + 0.2235|6, 0\rangle, \\
\text{Yb}^{3+} |\pm\rangle &= -0.256|3.5, \pm 3.5\rangle \pm 0.389|3.5, \pm 0.5\rangle \\
&\quad + 0.885|3.5, \mp 2.5\rangle. \tag{3}
\end{aligned}$$

Firstly, it is clear that the ground state of  $\text{Tm}^{3+}$  is a singlet due to its non-Kramers character, while for spin ice, a doublet ground state is required. For the remaining compounds where a doublet CEF ground state is realized, spins in  $\text{CdDy}_2\text{Se}_4$  and  $\text{CdYb}_2\text{Se}_4$  exhibit Heisenberg-like character, with  $g$ -factors of  $g_\perp = 5.69$ ,  $g_\parallel = 6.38$  for  $\text{Dy}^{3+}$  and  $g_\perp = 2.16$ ,  $g_\parallel = 3.97$  for  $\text{Yb}^{3+}$ . For the  $\text{Ho}^{3+}$  spin, an Ising character with  $g_\perp = 0$ ,  $g_\parallel = 4.43$  is observed, which satisfies the local Ising condition to realize the spin ice state. Therefore, from the CEF point of

view,  $\text{CdHo}_2\text{Se}_4$  might be the most promising compound to realize the quantum spin liquid state. However, it should be noted that the lowest CEF excited states in  $\text{CdDy}_2\text{Se}_4$ ,  $\text{CdTm}_2\text{Se}_4$ , and  $\text{CdHo}_2\text{Se}_4$  are lying at energies below  $\sim 2$  meV. Such low-lying excited levels might renormalize the spin couplings and make our single-ion analysis inappropriate [S4, S10].

### Dipolar spin ice state in $\text{CdEr}_2\text{S}_4$

Ice-correlations similar to that of  $\text{CdEr}_2\text{Se}_4$  are also observed in  $\text{CdEr}_2\text{S}_4$ . Fig. S4 presents the non-polarized neutron diffuse scattering results for  $\text{CdEr}_2\text{S}_4$  measured on DMC at PSI with the setup of 2.46 Å incoming neutron wavelength. The 50 K measurement has been subtracted as the background. Similar to the  $\text{CdEr}_2\text{Se}_4$  results shown in Fig. 2 of the main text, broad peaks at  $\sim 0.6$ , 1.4, and 2.5 Å<sup>-1</sup> are observed at low temperatures, which suggest similar ice-correlations in  $\text{CdEr}_2\text{S}_4$ .

Mean-field calculations were performed to confirm the ice-correlations in  $\text{CdEr}_2\text{S}_4$  [S11]. Denoting the  $\alpha$  component ( $\alpha = x, y, z$ ) of the  $\nu$ -th unit-length spin ( $\nu = 1, 2, 3, 4$ ) in the  $n$ -th primitive unit cell as  $S_{n,\nu,\alpha}$ , the Hamiltonian on the pyrochlore lattice can be explicitly expressed as:

$$\begin{aligned}
\mathcal{H} &= -E_a \sum_{n,\nu} \left[ (\hat{n}_\nu \cdot S_{n,\nu})^2 - |S_{n,\nu}|^2 \right] - J_1 \sum_{\langle n,\nu;n',\nu' \rangle} S_{n,\nu} \cdot S_{n',\nu'} \\
&\quad + Dr_0^3 \sum_{\langle n,\nu;n',\nu' \rangle} \left[ \frac{S_{n,\nu} \cdot S_{n',\nu'}}{|r_{n,\nu;n',\nu'}|^3} - \frac{3(S_{n,\nu} \cdot r_{n,\nu;n',\nu'})(S_{n',\nu'} \cdot r_{n,\nu;n',\nu'})}{|r_{n,\nu;n',\nu'}|^5} \right] \\
&= - \sum_{n,\nu,\alpha;n',\nu',\beta} J_{n,\nu,\alpha;n',\nu',\beta} S_{n,\nu,\alpha} S_{n',\nu',\beta}, \tag{4}
\end{aligned}$$

where the  $E_a$  term represents the easy-axis anisotropy and  $\hat{n}_\nu$  is the unit vector along the easy axis of the  $\nu$ -th spin. Fourier transform of the real-space coupling  $J_{n,\nu,\alpha;n',\nu',\beta}$  leads to the  $12 \times 12$  coupling matrix  $J_{k;\nu,\alpha;\nu',\beta}$  in reciprocal space, which is then diagonalized:

$$\sum_{\nu',\beta} J_{k;\nu,\alpha;\nu',\beta} u_{k;\nu',\beta}^{(\rho)} = \lambda_k^{(\rho)} u_{k;\nu,\alpha}^{(\rho)}, \tag{5}$$

where  $\lambda_k^{(\rho)}$  with  $\rho = 1, 2, \dots, 12$  denotes the eigenvalues and  $u_k^{(\rho)}$  denotes the corresponding eigenvectors. The global maximum of  $\lambda_k^{(\rho)}$  determines the long-range order transition under the mean-field approximation, with the transition temperature  $T_c$  as:

$$k_B T_c = \frac{2}{3} [\lambda_k^{(\rho)}]_{\max}$$

The paramagnetic susceptibility at  $T_{\text{MF}} > T_c$  can be approximated by the eigenvalues and eigenfunctions:

$$\chi_{k;\nu,\alpha;\nu',\beta} = \frac{N\mu^2}{V} \sum_{\rho} \frac{u_{k;\nu,\alpha}^{(\rho)} u_{k;\nu',\beta}^{(\rho)*}}{3k_B T_{\text{MF}} - 2\lambda_k^{(\rho)}}, \tag{6}$$

where  $N$  is the total number of the unit cell,  $V$  is the volume of the system, and  $\mu$  is the size of the magnetic moment. The cross section of the magnetic scattering can be expressed as:

$$\begin{aligned}
\frac{d\sigma}{d\Omega}(Q = \tau + k) &= Pf(Q)^2 k_B T \sum_{\alpha,\beta,\nu,\nu'} \left( \delta_{\alpha\beta} - \hat{Q}_\alpha \hat{Q}_\beta \right) \\
&\quad \times \chi_{k;\nu,\alpha;\nu',\beta} \cos[\tau \cdot (r_\nu - r_{\nu'})] - Kf(Q)^2, \tag{7}
\end{aligned}$$

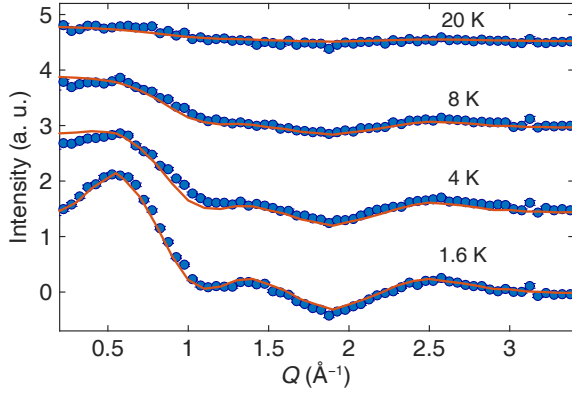


FIG. S4. Non-polarized neutron diffuse scattering results for  $\text{CdEr}_2\text{S}_4$  measured at 1.6, 4, 8, and 20 K with the 50 K data subtracted as the background. The data at 4, 8, and 20 K are shifted by 1.5, 3.0, and 4.5 along the  $y$  axis, respectively. The mean-field calculation results assuming only dipolar interactions are shown as the solid lines.

where  $P$  is a constant,  $f(Q)$  is the magnetic form factor,  $\tau$  is the reciprocal lattice vector, and  $r_\nu$  denotes the position of the  $\nu$ -th atom in the first primitive cell. The additional term of  $Kf(Q)^2$  accounts for the subtracted spin correlations at 50 K.

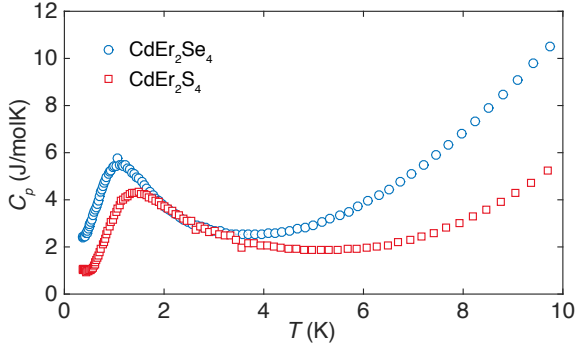


FIG. S5. Specific heat for  $\text{CdEr}_2\text{Se}_4$  and  $\text{CdEr}_2\text{S}_4$  single crystals. Tails at the lowest temperature might be due to impurities.

To account for the Ising character of the  $\text{Er}^{3+}$  spin, a high anisotropy of  $E_a = 100$  K was used. The dipolar interactions with  $D = 0.69$  K was truncated beyond the length of 5 unit cells. Since  $T_c$  is an effective temperature that can be different from the real ordering temperature, the mean-field temperature  $T_{\text{MF}}$  was used as a fitting parameter [S11]. Fig. S4 presents the fitted results with  $J_1 = 0$ . In this case,  $T_c$  is calculated to be 1.8 K, and the fitted  $T_{\text{MF}} = 1.9, 2.3, 3.8,$  and  $15.8$  K for the data measured at 1.6, 4, 8, and 20 K, respectively. Thus the ice-correlation is proved to exist in  $\text{CdEr}_2\text{S}_4$ .

In our mean-field calculation, the variance of  $J_1$  does not affect the goodness-of-fit as long as  $J_1/3 + 5D/3 > 0$ . To obtain the monopole chemical potential, we measured

the specific heat  $C_p$  for  $\text{CdEr}_2\text{S}_4$  single crystals. As is shown in Fig. S5, the  $C_p(T)$  maximum of  $\text{CdEr}_2\text{S}_4$  is at  $\sim 1.4$  K, which enable us to fix the monopole chemical potential to 3.84 K in  $\text{CdEr}_2\text{S}_4$  (see main text).

### Freezing and ordering temperatures in $\text{CdEr}_2\text{Se}_4$

The true ground state of a dipolar spin ice has again become a topical question [S12]. An ordering transition is expected due to the bandwidth of the dipolar spin ice microstates [S13], the transition temperature and eventual ground state being controlled by  $D/J_2$  [S14–S16]. In  $\text{Dy}_2\text{Ti}_2\text{O}_7$  a transition to *antiferromagnetic* order is expected at  $\sim 0.1$  K [S15–S17], far below temperatures at which equilibration is easily possible, *i.e.* 0.65 K [S18].

The freezing temperature of 0.29 K for  $\text{CdEr}_2\text{Se}_4$  is estimated from the 0.65 K freezing temperature of  $\text{Dy}_2\text{Ti}_2\text{O}_7$ . With the known monopole parameters, the temperature dependence of the monopole density  $\rho(T)$  can be obtained using the Debye-Hückel theory [S19]. Assuming the monopole hopping rate  $u$  to be temperature independent and  $u\rho$  to be the same at the freezing temperature for  $\text{CdEr}_2\text{Se}_4$  and  $\text{Dy}_2\text{Ti}_2\text{O}_7$ , we first calculate the monopole density in  $\text{Dy}_2\text{Ti}_2\text{O}_7$  at 0.65 K, then divide by 100 to account for the increased value of  $u$  in  $\text{CdEr}_2\text{Se}_4$ , and finally locate the freezing temperature in  $\text{CdEr}_2\text{Se}_4$  by following its  $\rho(T)$  relation using Debye-Hückel theory.

The ordering temperature  $T_c = 0.37$  K for  $\text{CdEr}_2\text{Se}_4$  is estimated from the  $J_2/D$ - $T_c/D$  phase diagram in Ref. [S20]. Considering the  $-3$  times difference in the definition of  $J_2$ , the ratio  $J_2/D$  is found to be  $-0.2$ , which leads to  $T_c = 0.37$  K under a linear extrapolation of the boundary between the classical spin ice and ferromagnetically long-range ordered phases. This means that in  $\text{CdEr}_2\text{Se}_4$  there is a chance not only to investigate a spin ice with an alternative ground state; but also to study the effect on monopole dynamics of reaching a temperature comparable to the bandwidth of the spin ice states where new monopole-monopole interaction terms may appear.

### Note for the ground state doublet splitting in $\text{Dy}_2\text{Ti}_2\text{O}_7$

Private communications with the authors of Ref. [S21] confirm a typo for the fitted parameter  $\alpha$  in Eq. (9) of their publication. The correct value should be  $\alpha = 3.29 \times 10^{-6}$  [meV/T<sup>3</sup>], which we reproduce using the same CEF parameters. The similar but different values of  $\alpha = 2.14 \times 10^{-6}$  [meV/T<sup>3</sup>] and  $A = 0.183$  reported in our main text are calculated with refined CEF parameters [S22], which were not available to the authors of Ref. [S21].

- 
- \* oksana.zaharko@psi.ch  
† tom.fennell@psi.ch
- [S1] S. Calder and T. Fennell and W. Kockelmann and G. C. Lau and R. J. Cava and S. T. Bramwell, *J. Phys. Condens. Matter* **22**, 116007 (2010).
- [S2] J. Lago, I. Živković, B. Z. Malkin, J. Rodriguez Fernandez, P. Ghigna, P. Dalmas de Réotier, A. Yaouanc, and T. Rojo, *Phys. Rev. Lett.* **104**, 247203 (2010).
- [S3] G. C. Lau, R. S. Freitas, B. G. Ueland, P. Schiffer, and R. J. Cava, *Phys. Rev. B* **72**, 054411 (2005).
- [S4] A. Yaouanc, P. Dalmas de Rotier, A. Bertin, C. Marin, E. Lhotel, A. Amato, and C. Baines, *Phys. Rev. B* **91**, 104427 (2015).
- [S5] D. Yoshizawa, T. Kida, S. Nakatsuji, K. Iritani, M. Halim, T. Takeuchi, and M. Hagiwara, *App. Mag. Res.* **46**, 993 (2015).
- [S6] T. Higo, K. Iritani, M. Halim, W. Higemoto, T. U. Ito, K. Kuga, K. Kimura, and S. Nakatsuji, *Phys. Rev. B* **95**, 174443 (2017).
- [S7] Bertin A. and Chapuis Y. and Dalmas de Réotier P. and Yaouanc A., *J. Phys. Condens. Matt.* **24**, 256003 (2012).
- [S8] A. Freeman and J. Desclaux, *J. Mag. Mag. Mater.* **12**, 11 (1979).
- [S9] J. Jensen and A. R. Mackintosh, *Rare Earth Magnetism* (Clarendon Press, Oxford, 1991).
- [S10] H. R. Molavian, M. J. P. Gingras, and B. Canals, *Phys. Rev. Lett.* **98**, 157204 (2007).
- [S11] H. Kadowaki, Y. Ishii, K. Matsuhira, and Y. Hinatsu, *Phys. Rev. B* **65**, 144421 (2002).
- [S12] D. Pomaranski, L. R. Yaraskavitch, S. Meng, K. A. Ross, H. M. L. Noad, H. A. Dabkowska, B. D. Gaulin, and J. B. Kycia, *Nat. Phys.* **9**, 353 (2013).
- [S13] R. G. Melko, B. C. den Hertog, and M. J. P. Gingras, *Phys. Rev. Lett.* **87**, 067203 (2001).
- [S14] J. P. C. Ruff, R. G. Melko, and M. J. P. Gingras, *Phys. Rev. Lett.* **95**, 097202 (2005).
- [S15] P. A. McClarty, O. Sikora, R. Moessner, K. Penc, F. Pollmann, and N. Shannon, *Phys. Rev. B* **92**, 094418 (2015).
- [S16] P. Henelius, T. Lin, M. Enjalran, Z. Hao, J. G. Rau, J. Altosaar, F. Flicker, T. Yavors’kii, and M. J. P. Gingras, *Phys. Rev. B* **93**, 024402 (2016).
- [S17] T. Yavors’kii, T. Fennell, M. J. P. Gingras, and S. T. Bramwell, *Phys. Rev. Lett.* **101**, 037204 (2008).
- [S18] J. Snyder, B. G. Ueland, J. S. Slusky, H. Karunadasa, R. J. Cava, and P. Schiffer, *Phys. Rev. B* **69**, 064414 (2004).
- [S19] H. D. Zhou, S. T. Bramwell, J. G. Cheng, C. R. Wiebe, G. Li, L. Balicas, J. A. Bloxsom, H. J. Silverstein, J. S. Zhou, J. B. Goodenough, and J. S. Gardner, *Nat. Commun.* **2**, 478 (2011).
- [S20] P. A. McClarty, O. Sikora, R. Moessner, K. Penc, F. Pollmann, and N. Shannon, *Phys. Rev. B* **92**, 094418 (2015).
- [S21] B. Tomasello, C. Castelnovo, R. Moessner, and J. Quintanilla, *Phys. Rev. B* **92**, 155120 (2015).
- [S22] M. Ruminy, E. Pomjakushina, K. Iida, K. Kamazawa, D. T. Adroja, U. Stuhr, and T. Fennell, *Phys. Rev. B* **94**, 024430 (2016).